# MuxHand: A Cost-Effective and Compact Dexterous Robotic Hand Using Time-Division Multiplexing Mechanism

Jianle Xu[1*], Shoujie Li[1*], Hong Luo[1], Houde Liu[1†], Xueqian Wang[1], Wenbo Ding[1], Chongkun Xia[2]

***Abstract*— The number of motors directly influences the dexterity, size, and cost of a robotic hand. In this paper, we present MuxHand, a robotic hand that utilizes a time-division multiplexing motor (TDMM) mechanism. This system enables independent control of 9 cables with just 4 motors, significantly reducing both cost and size while maintaining high dexterity. To enhance stability and smoothness during grasping and manipulation tasks, we integrate magnetic joints into the three 3D-printed fingers. These joints provide impact resistance, resetting capabilities. The three fingers together have a total of 30 degrees of freedom (DOF), 18 of which are passive DOF, allowing the hand to conform closely to the surface of an object during grasping. We conduct a series of experiments to assess the performance parameters of MuxHand, including its grasping and manipulation capabilities. The results show that the TDMM mechanism precisely controls each cable connected to the finger joints, enabling robust grasping and dexterous manipulation. Furthermore, compared to the traditional approach of assigning a motor to each active DOF, the cost is reduced by 42.06%. The maximum load of a single finger reaches 7.0 kg, the maximum load at the finger joint root is 12.0 kg, the maximum driving force at the joint root is 5.0 kg, and the maximum fingertip force is 10.0 N.**

## I. Introduction

The robotic hand, as a general end-effector for humanoid robots, performs both grasping [1], [2] and dexterous manipulation tasks [3]. Numerous advanced dexterous hands have been developed , such as the DLR/HIT Hand [4], the ILDA Hand [5], the RoboRay Hand [6], and others [7]–[9]. These hands generally have a high active degree of freedom (DOF). However, an increased DOF often requires more motors, which results in a larger size, greater weight and higher cost.

To overcome these limitations, Kontoudis *et al*. [10] and Baril *et al*. [11] introduce mechanisms that utilizes mechanical selectors to connect or disconnect a motor from a specific cable, Kim *et al*. proposed a switchable cable-driven (SCD) mechanism that uses multiple electrostatic clutches to individually control several cables with a single motor. These approaches use mechanisms that switch a single motor to control the connection of the required cables, allowing for independent control of the DOF, which reduces cost and size. However, they rely on manual switching or the friction of electrostatic clutches, which limits their potential for broader application.

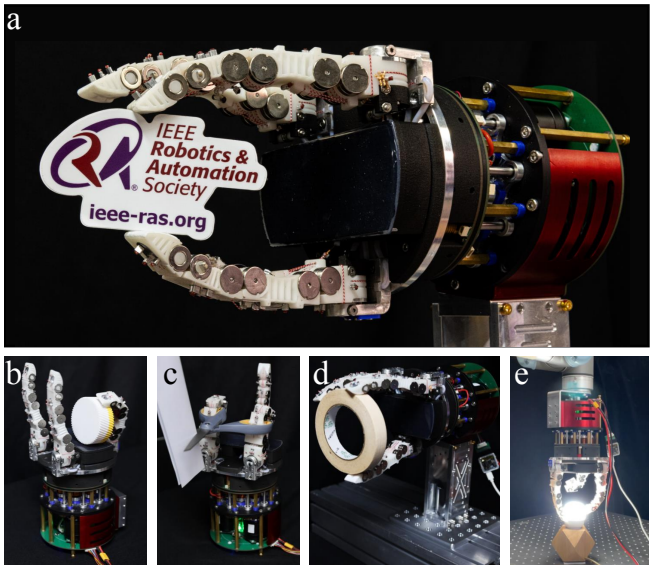


Fig. 1. MuxHand prototype. (a) MuxHand pinching a piece of paper. (b) Single finger operating a disc. (c) Two fingers using scissors to cut paper. (d) Three fingers rotating a ring. (e) Two fingers screw the light bulb into the socket.

In this paper, we present MuxHand, a robotic hand that utilizes the time-division multiplexing motor (TDMM) mechanism to control the 9 DOF of its three fingers with just 4 motors, reducing both cost and size compared to traditional approaches. As shown in Fig. 1, the prototype of MuxHand and its dexterous manipulation capabilities are demonstrated. Its three 3D-printed fingers, equipped with magnetic joints, provide 18 additional passive DOF, enabling the hand to not only perform robust grasping and dexterous manipulation tasks but also feature self-resetting and impact-resistant properties. The contributions of our work are as follows:

- We design a cable-driven robotic hand based on the TDMM mechanism, using only 4 motors to control 9 DOF for grasping and dexterous manipulation. Compared to a system using 9 motors with identical individual motor performance, our design reduces 42.06% cost and minimizes size.
- We design a mechanism with switchable motor output positions, allowing the deployment of a few high-power

∗ These authors contributed equally to this work.

This work was supported by the National Natural Science Foundation of China (92248304), Shenzhen Science Fund for Distinguished Young Scholars (RCJC20210706091946001), Shenzhen Science and Technology Program (JCYJ20220530143013030) and Shenzhen Higher Education Stable Support Program (WDZC20231129093657002).

1 Jianle Xu, Shoujie Li, Hong Luo, Wenbo Ding, Houde Liu, and Xueqian Wang are with Shenzhen International Graduate School, Tsinghua University, Shenzhen 518055, China.

2 Chongkun Xia is with School of Advanced Manufacturing, Sun Yat-sen University, shenzhen 518107, China

† Corresponding authors: Houde Liu (liu.hd@sz.tsinghua.edu.cn).

This paper has supplementary material available at https://xujianle.github.io/MuxHand.github.io.

motors within a limited size. Compared to deploying an equal number of small-power motors for each DOF within the same size, this design ensures independent control while increasing the output torque by over 200%.
- We design a cable-driven finger with magnetic joints, offering 18 passive DOF, impact resistance, and resetting capabilities. The joints misalign passively for better object conformity, while the self-locking mechanism maintains grip during power loss.
- We validate the grasping and manipulation capabilities of MuxHand through a series of experiments and measure its detailed performance parameters.

The rest of the paper is structured as follows: The related works is reviewed in Section II. In Section III, we describe the drive box design, the principle of the transmission mechanism, and the finger module design, along with an analysis of the kinematic relationship between the finger joints and the winding wheels. In Section IV we present the experimental setup, the experimental results obtained. In Section V, we discuss the overall advantages and innovations of the MuxHand, and finally in Section VI, we conclude the paper.

## II. Related Works

The robotic hand is mainly divided into fully actuated dexterous hands and underactuated dexterous hands. For a fully actuated dexterous hand, the number of actuators is equal to the number of DOF [4], [5], [12], [13]. Due to their high number of DOF, these hands exhibit high flexibility, enabling them to perform not only grasping tasks but also complex manipulation tasks. However, they come with challenges such as increased size, weight, and cost due to the large number of motors required.

On the other hand, underactuated dexterous hands utilize fewer motors than the number of DOF, which often leads to reduced size, cost, and complexity. This type of design often incorporates mechanisms like mechanical coupling or compliant structures to achieve flexible control of multiple joints with fewer motors [14]–[17]. Several studies have attempted to optimize grasping performance by integrating rigid and flexible designs [18]–[27]. However, a major limitation of such systems is that, with a reduced number of DOF, individual joint control is difficult, making dexterous manipulation challenging.

To overcome these limitations, the MuxHand we designed is capable of independently controlling 9 DOF across three fingers with only 4 motors. It not only enables robust grasping but also performs dexterous manipulation tasks. Compared to traditional fully actuated solutions, it reduces cost and minimizes size.

## III. Mechanical Design And Evaluation

In this section, we describe the structure of MuxHand and provide an analysis of its design. The MuxHand, as shown in Fig. 2a, has a diameter of 120 mm and a height of 264 mm. It consists of the drive box, winding wheel module, and finger module.

### A. Drive Box Design

The TDMM mechanism is driven by an axial motor, which activates several radial motors to rotate and switch to the required output positions. To maximize the output torque within the limited volume, an HTM4538 axial motor is employed, while the radial motors consist of three MF4015 units.

To achieve a more compact structure, three highly integrated PCB are designed, as shown in Fig. 2d. PCB1 is the main control PCB, which manages the entire hardware system, handles communication with other boards and sensors, as well as task planning and power conversion. It supports up to 60V direct current (DC) input and uses the STM32F446-RET6 Microcontroller Unit (MCU) with a 180 MHz frequency. To prevent the wires supplying power and communication signals to the radial motors from tangling due to axial rotation, a conductive slip ring structure (comprising PCB2 and PCB3) is designed. This ensures uninterrupted power and communication to the motors. The gear module, consisting of 9 gear groups, transmits the torque from the radial motors, while the coil module, made of 9 enameled wire coils and a control PCB, manages the connection and disconnection of the motor's torque.

In the drive box, power and signals are transmitted between the PCB and the modules through copper columns, which function both as structural supports and electrical connectors. This dual role enhances the system's load capacity and stability. To facilitate communication with each component, the CAN protocol [28] is utilized, operating at a rate of 1.0 Mbits/s.

### B. Winding wheel module design

As shown in Fig. 2e, the winding wheel module integrates 9 sets of winding wheels used to wrap the drive cables for controlling the finger joints. These wheels are driven by a worm gear and worm screw, providing self-locking capability to ensure that the winding wheels do not shift even when power is lost. To monitor the current rotational angle of the winding wheels, we have designed and integrated a magnetic encoder (PCB4) at the end of the winding wheel shaft. The encoder chip we use is AS5047P, which offers a 14-bit resolution with a range from 0 to 16,383. All magnetic encoder are connected to the decoder board (PCB5) using 0.5 mm pitch FPC cables [28]. Each magnetic encoder communicates with the decoder board via the Serial Peripheral Interface (SPI) protocol at a baud rate of 9.0 Mbits/s. Once the decoder board collects the angle data, its MCU transmits the data to the CAN bus.

### C. TDMM Mechanism and Transmission Mechanism

The core concept of the TDMM mechanism is to control the movement of multiple radial motors using a time-division multiplexing (TDM) approach. By leveraging the TDM principle, control tasks for multiple DOF are assigned to a limited

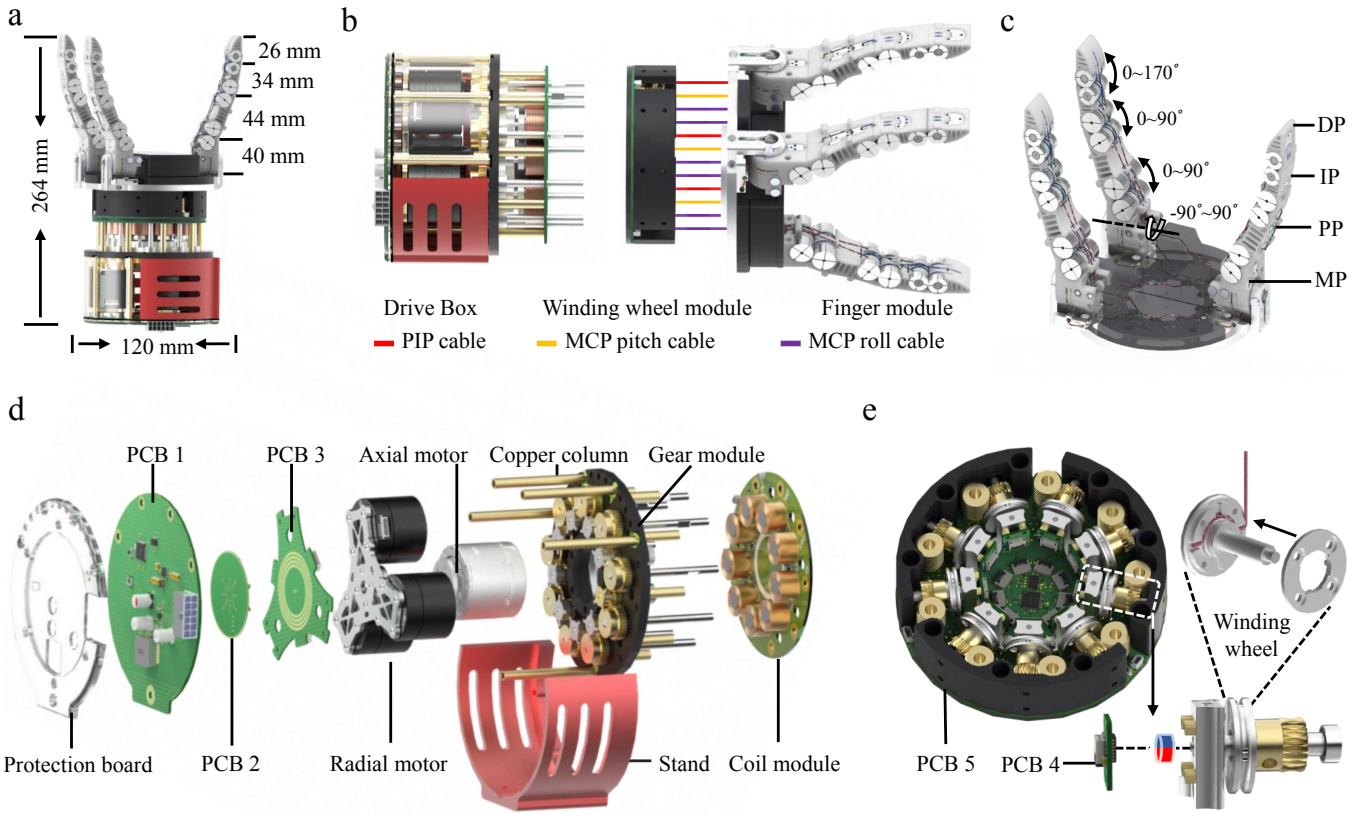


Fig. 2. MuxHand system overview. (a) MuxHand dimensions. (b) Main structure of MuxHand. (c) Structure of the finger module. (d) Exploded view of the drive box. (e) Structure of the winding wheel module.

number of motors, with each motor controlling multiple cables during specific time slots. Despite the reduced number of motors, precise scheduling and timing control enable accurate regulation of multiple DOF within constrained space and cost. Additionally, the use of fewer motors allows for the incorporation of larger motors, resulting in higher torque output.

The process is as follows: The axial motor rotates the three radial motors to different positions, as shown in Fig. 3(a), which illustrates the radial motors' state. The Radial motors includes Motor 1, Motor 2, and Motor 3. In Fig. 3a, different colors represent different motors, and varying shades of the same color indicate the positions of each motor at different times. Experimental validation shows that the switching time per cycle is 0.18 seconds, while the transmission connection time is 0.37 seconds. As shown in Fig. 3b, Initially, when no current flows through the electromagnetic coil, the iron core is not magnetized but still attracts the plug, which has a magnet attached to it. Once the radial motor group reaches the target position, as shown in Fig. 3c, the electromagnetic coil at this position is energized in a fixed direction, causing the iron core to become magnetized. According to the right-hand rule, the magnetic polarity of the iron core is determined. The attached magnet on the plug is then lifted by the repulsive force from the magnetized iron core, aligning the gear component with the motor output slot. As a result, the torque output by the radial motor is transmitted through the gear module and winding wheel module, ultimately reaching the winding wheel.

During this process, Proportional-Integral-Derivative (PID) control algorithms [29] are employed for closed-loop speed and position control to drive the axial motor to different positions. However, some mechanical error inevitably arises between the torque transmission slots and plugs. As shown in Fig. 3a, after the plug is lifted into the slot, the maximum error between the slot and plug is approximately 10°. This error occurs at the radial motor, but when translated to the winding wheel, it must be compensated for through the reduction gears. Based on the number of teeth on the gears $Z_1, Z_2, Z_4$ and the number of threads on the helical gear $Z_3$ in Fig. 3.c, the transmission reduction ratio $k$ can be calculated as follows:

$$k = \frac{Z_2 \cdot Z_4}{Z_1 \cdot Z_3}. \tag{1}$$

The final calculated reduction ratio is 33.33, which results in a maximum error of only 0.30° when apply to the winding wheel. The maximum error applied to the driving cable is only 0.044 mm, resulting in a very small impact on finger movement.

### *D. Finger Module Design*

As shown in Fig. 2c, the finger module consists of three anthropomorphic fingers, each with four phalanges: the distal phalanx (DP), intermediate phalanx (IP), proximal phalanx (PP), and metacarpal phalanx (MP). The joints between the fingers are connected using decoupled rolling joints, ensuring

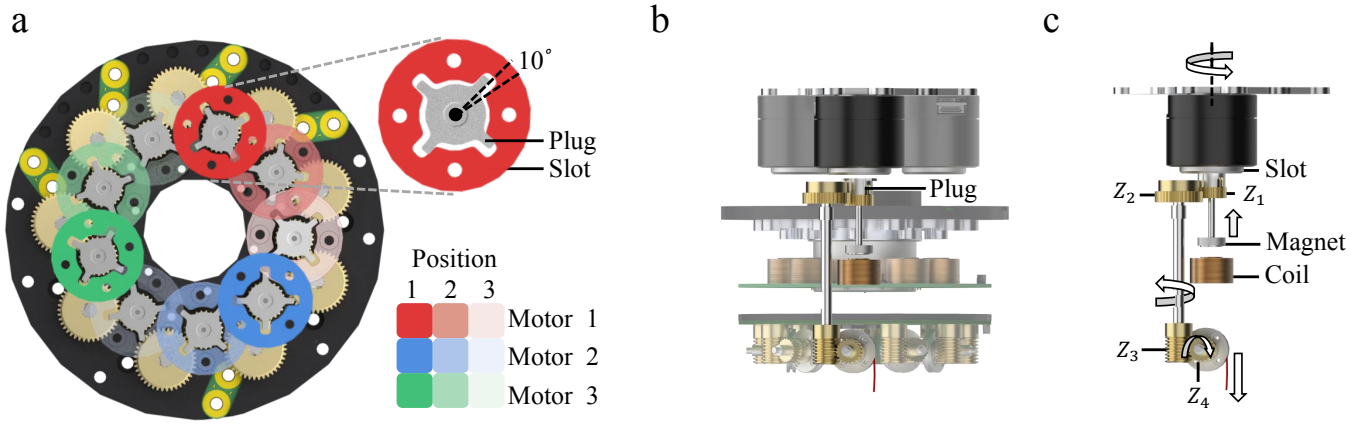


Fig. 3. TDMM mechanism and transmission mechanism. (a) Operating positions of the radial motor group at different times. Different colors represent individual motors, with varying shades of the same color indicating the motor positions at different time points. (b) Initial state of the transmission mechanism when the radial motor reaches its position. (c)Torque transmission from the radial motor to the winding wheel. $Z_1, Z_2, Z_3, Z_4$ represent the number of teeth on the gears, where $Z_1 = 24, Z_2 = 40, Z_3 = 1$, and $Z_4 = 20$.

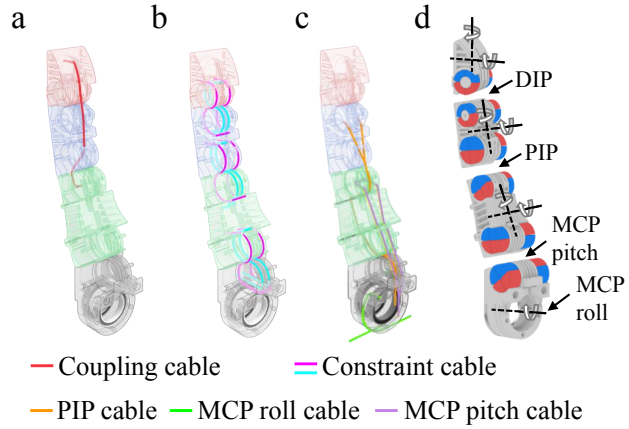


Fig. 4. Structure of single finger. (a) DIP joint and PIP joint coupling cable. (b) Constraint cables between the joints of each finger. (c) The orange cable represents the PIP joint drive, yellow is for the MCP pitch joint drive, and green is for the MCP roll joint drive. (d) Arrangement of magnetic joints

independent movement of each joint [30]. These four joints correspond to the four DOF of a single finger. Of these DOF, three are actively controlled, while the remaining one is coupled with the Proximal Interphalangeal (PIP) joints. The entire finger is 3D printed using photosensitive resin material, and each finger's joints are cable-driven. To reduce weight while maintaining strength, the fingers feature a hollowed-out structure. In a cable-driven system, minimizing friction between the cable and its constraints is crucial for improving transmission efficiency and output force [31]. To achieve this, polytetrafluoroethylene (PTFE) tubing, known for its low coefficient of friction [32], is installed at key positions.

The finger consists of three types of cables: coupling cables (Fig. 4a), constraint cables (Fig. 4b), and drive cables (Fig. 4c). The coupling cables allow the Distal Interphalangeal (DIP) joint to rotate synchronously with the PIP joint at a specific ratio [33], mimicking the movement of a human finger. Constraint cables are used to restrict and connect the various finger joints, while drive cables are used to actuate the joints. Since all drive cables must pass through the MetaCarpoPhalangeal (MCP) roll joint, it is crucial to ensure that there is no interference between the cables during finger joint movements and no coupling effects between the drive joints. Therefore, the cable routing needs to be decoupled to prevent interference with the movement of other joints. Fig. 4c illustrates the position of each driving cable. However, merely having joint constraint cables and drive cables is not enough; the fingers need additional forces to reset. As shown in Fig. 4d, we integrate radially magnetized magnets at each joint, which not only provide resetting torque for the joints but also offer an additional two passive DOF for each joint. The red parts indicate the north pole, and the blue parts indicate the south pole. This allows the fingers to passively adjust their posture based on the object being grasped, enabling better wrapping around the object surface or resistance to external impacts.

To achieve precise control of finger movement, we established the relationship between the finger joint motion and the winding wheel motion.

Fig. 5a illustrates the schematic of the coupling relationship between the DIP joint and PIP joint, where the $r_1$ and $r_2$ are the radii of the rolling joints of the DIP joint and PIP joint, respectively, and the $r_3$ is the radius of the winding wheel. The yellow line in Fig. 5a is the drive cable for the PIP joint. The change in length of this cable caused by the winding wheel is denoted as $\Delta x_2$. When the winding wheel rotates by an angle $\varphi_1$, $\Delta x_2$ is given by:

$$\Delta x_2 = \varphi_1 \cdot r_3. \tag{2}$$

Since the PIP drive cable is fixed in the intermediate phalanges and is constrained to be tangent to the rolling joint surface of the proximal phalanges, the rotation angle of the PIP joint $\theta_2$ can be derived from geometric relationships as:

$$\theta_2 = 2\alpha_2. \tag{3}$$

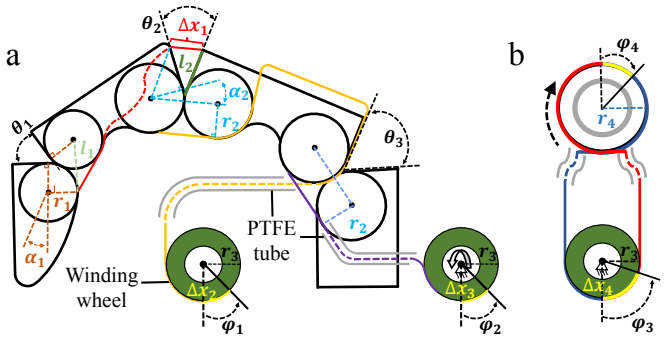


Fig. 5. The schematic of the relationship between the finger joints and the winding wheel motion. (a) The relationship between the DIP, PIP, MCP pitch joints and the winding wheel motion. (b) The relationship between the MCP roll and winding wheel.

Here, $l_2$ can be determined as:

$$l_2 = \sqrt{r_2^2 + (2r_2 - \Delta x_2)^2}, \tag{4}$$

where $\alpha_2$ is the angle of rotation of the virtual link of the proximal phalanges relative to the PIP joint, given by:

$$\alpha_2 = \arcsin(\frac{5r_2^2 - l_2^2}{4r_2^2}). \tag{5}$$

Substituting $l_2$ into this with (4),

$$\theta_2 = 2\alpha_2 = 2\arcsin[\frac{\Delta x_2}{r_2} - (\frac{\Delta x_2}{2r_2})^2], \tag{6}$$

with $\theta_2$, the change in length of the coupling cable $\Delta x_1$, as shown in Fig. 7(a), can be calculated. This change determines the rotation angle of the DIP joint:

$$\Delta x_1 = 2l_2 \sin(\alpha_2). \tag{7}$$

Using a similar method, the rotation angle of the DIP joint $\theta_1$ can be calculated as:

$$\theta_1 = 2\alpha_1 = 2\arcsin[\frac{\Delta x_1}{r_1} - (\frac{\Delta x_1}{2r_1})^2]. \tag{8}$$

The calculation method for the MCP pitch joint is similar to that for the PIP joint. The calculation method for the MCP roll joint's rotation angle relative to the winding wheel's rotation angle differs slightly from that of the other joints. As shown in Fig. 5b, when the winding wheel rotates by a certain angle, the MCP roll joint experiences the same arc length displacement, resembling the motion of a pair of gears. Therefore, without accounting for cable tension, this motion follows a completely linear relationship.

Fig. 6a shows the relationship between the winding wheel's rotation and the DIP, PIP joints, while Fig. 6b illustrates the relationship between the winding wheel's rotation angle and the MCP pitch, MCP roll joints. We fit these relationships using linear regression equations, revealing a linear correlation between the rotation angles of the DIP and PIP joints and the winding wheel, ensuring smooth operation of the finger joints.

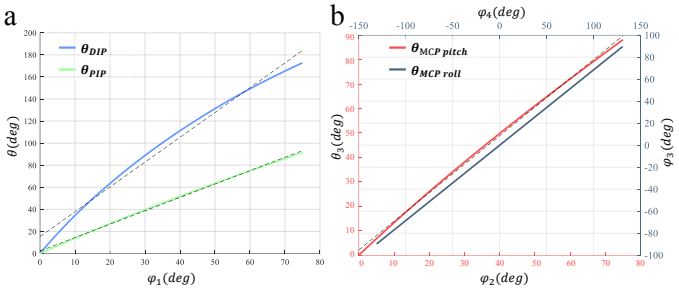


Fig. 6. The relationship between the winding wheel and each joint. (a) The relationship between $\theta_{DIP}$, $\theta_{PIP}$ and $\theta_{\varphi}$ is determined and fitted using a linear regression equation. (b) The relationship between $\theta_{MCP_{pitch}}$, $\theta_{MCP_{roll}}$ and $\theta_{\varphi}$

.

## IV. Experiments and Results

In this section, we present grasping and in-hand manipulation experiments to demonstrate the MuxHand's performance. Due to the flexibility of the MuxHand's fingers, all experiments use hard-coded methods for position control. Additionally, we conduct tests to evaluate the finger's load capacity and impact resistance. The overall parameters of the MuxHand are presented in Table I.

### A. Grasping Experiments

The first experiment focus on the MuxHand's ability to grasp objects. We select various objects from the YCB object set [34] and common objects in daily life. The YCB object set is a widely recognized benchmark dataset for evaluating robotic grasping, manipulation, and object recognition. Twelve objects are tested, as shown in Fig. 7 (a)-(l), including a cracker box, foam brick, USB hub, can of chips, apple, metal mug, thermometer, wine glass, lighter, dice, mustard container, and ice-cream stick, with their respective labels in Fig. 7(a)–(l).

Due to the MuxHand's 3 active DOF per finger, it is capable of grasping objects in a variety of ways. The MuxHand can use two fingers to pinch objects or employ three fingers to clip or wrap them. For tiny objects that cannot be enveloped in the hand's palm, the MCP roll joints of two fingers move toward each other in opposite directions, allowing the fingertips to precisely aim at the object. When grasping longer objects like ice-cream sticks, a three-finger method ensures stability. For heavier and larger objects, an enveloping grasp can be used, where the fingers and palm enclose the entire object to ensure a stable hold. This flexibility in grasping strategies highlights the MuxHand's adaptability to a wide range of object sizes, shapes, and weights.

### B. Dexterous Manipulation Experiments

Beyond grasping, dexterous manipulation is crucial for dexterous hand. We conduct several experiments to validate the MuxHand's dexterous manipulation capabilities. As shown in Fig. 7(m)-(o), the objects used for these experiments include a disc, a pair of scissors, and a ring.

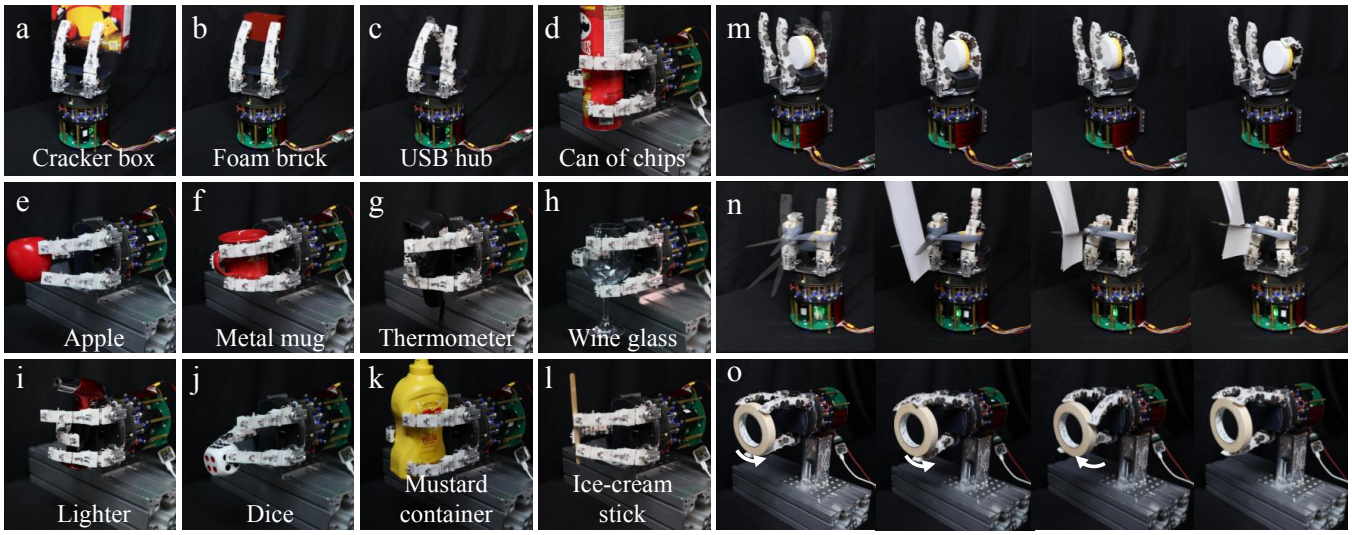


Fig. 7. Grasping and dexterous manipulation experiments. (a)–(l) are the objects selected for grasping experiments (m) The hand rolls a disc. (n) The hand uses a pair of scissors to cut a sheet of paper. (o) The hand rotates a ring to a specific angle.

TABLE I: MuxHand Overall Performance Parameters

| Items | Parameters |
|---|---|
| Weight (including motors) | 2.6 kg |
| Max. root payload (single finger) | 12.0 kg |
| Max. driving capability （root） | 5 kg |
| Max. payload (single finger) | 7.0 kg |
| Min. position switch time | 0.18 s |
| Min. transmission connection time | 0.37 s |
| Active DOF | 9 |
| Passive DOF | 21 |
| Dimension (H × L × W) | 264 mm × 120 mm × 120 mm |
| Motors | Axial motor (0.3 Nm) × 3<br>Radial motor (0.25 Nm) × 1 |
| Communication protocol | CAN @ 1Mbits/s |
| Maximum Power | 240 Watt @ 24 Volt |

In Fig. 7(m), the MuxHand uses its fingertip to press on a disc, rolling it back and forth within the palm. This demonstrates the hand's ability to finely adjust an object while maintaining continuous contact and control. In Fig. 7n, the MuxHand uses two fingers use a pair of cissors to cut a sheet of paper. The MuxHand first grasps the scissors, then rotates the MCP roll joint to open and close them. Due to the limited aperture of the scissors, the joints will experience lateral forces during finger operation. The designed fingers can accommodate these lateral forces through joint misalignment, allowing the cutting task to be completed without damaging the fingers. Once the lateral forces are no longer applied, the joints will reset automatically. As shown in Fig. 7(o), involves the MuxHand grasping a ring with its fingertips and rotating it. Fig. 8 shows the MuxHand performing a two-finger manipulation on a light bulb, using a pinch grip and side-swing motion to screw the bulb into the socket. Fig. 8a shows the initial state, and Fig. 8b demonstrates the light bulb successfully screwed into the socket and illuminated after two rotations.

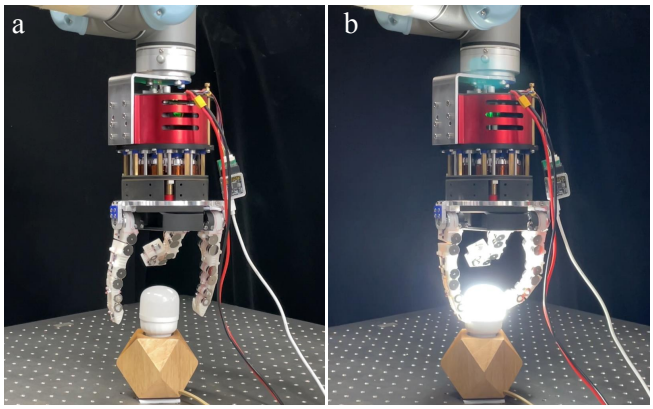


Fig. 8. Two-finger manipulation experiment. (a) Initial state. (b) Using two fingers to screw the light bulb into the socket.

### C. Load Experiments

In addition, we conduct load testing on the MuxHand. As shown in Fig. 9a, during the testing process, the motors are in a power-off state and provide no torque. Relying on the self-locking mechanism of the MuxHand, the maximum load capacity of a single finger reaches 7.0 kg. The MCP roll joint of the MuxHand is one of the key DOF for executing operations. Due to the finger's ability to resist impact displacement, we test the MCP roll joint at the base of the finger. The tests include maximum load testing and driving load testing. As shown in Fig. 9b, the maximum load capacity of the MuxHand MCP roll joint reaches 12.0 kg, while the maximum load it can drive, as shown in Fig. 9c, is 5 kg. Additionally, fingertip force testing is conducted (Fig. 9d), revealing a maximum load capacity of 1.0 kg. Finally, as shown in Fig. 9e, we perform impact resistance testing on the finger by repeatedly striking the moving finger with a hammer. The results show that no damage occurs during the test and the finger continues to function normally.

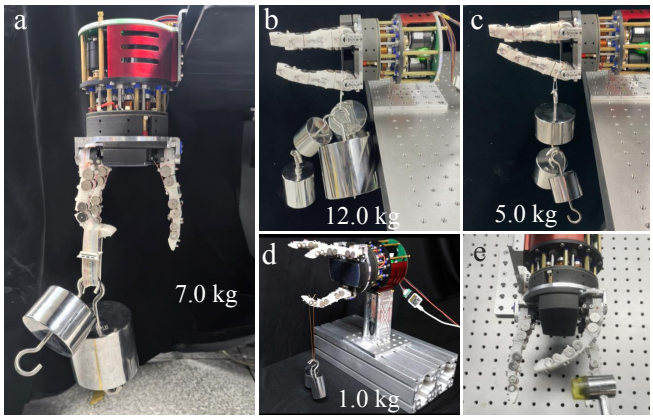


Fig. 9. Load Experiments. (a) Maximum load capacity of single finger. (b) Maximum load capacity of the MuxHand MCP roll. (c) Maximum driving Load of the MCP roll Joint. (d) Maximum fingertip driving force. (e) Impact resistance experiment.

TABLE II: Cost of System

| Type | Item | Num | Price |
|---|---|---|---|
| Motors | HTM4538 | 1 | $109.6 |
| | MF4015 | 3 | $222.27 |
| TDMM mechanism | Control board | 1 | $6.25 |
| | Ebamelled wire coils | 9 | $4.32 |
| Standard parts | Cylindrical gears | 18 | $14.82 |
| | Worm gears | 18 | $13.58 |
| | Pin shafts | 9 | $2.64 |
| | Copper columns | 14 | $0.55 |
| | Magnets | 51 | $8.52 |
| | Bearing | 33 | $10.5 |
| Non-standard parts | Aluminum alloy shell | 1 | $27.44 |
| | Support parts | 2 | $12.35 |
| | Finger wire end fixers | 12 | $14.41 |
| | 3D printed fingers | 3 | $8.23 |
| | Other materials | | $5 |
| Other components | Cable | | $0.27 |
| | Screws | | $0.55 |
| | PTFE tube | | $0.14 |
| **Total cost** | | | $461.44 |

## V. Discussion

We develop the MuxHand, with its key innovation being the combination of the TDMM mechanism and magnetic joint fingers. The TDMM mechanism (i.e., time-division multiplexing motors) is proposed for the first time in this work. This mechanism is particularly suitable for scenarios where space and cost are limited, but a large number of active DOF still need to be controlled. The MuxHand developed in this work effectively demonstrates this capability: by using only 4 motors, the MuxHand can control 9 DOF at different times, with a maximum of 3 DOF controlled simultaneously. Compared to traditional approaches that require 9 motors to drive 9 active DOF, this method saves 5 motors, reduces costs by 42.06%, and further minimizes the system's size, as shown in Table II, which presents the system's cost. Additionally, the introduction of magnetic joints provides each finger with an extra 6 passive DOF, significantly enhancing the finger's impact resistance and improving its adaptive ability when grasping objects.

## VI. Conclusion

In this paper, we present a cable-driven robotic hand named MuxHand, which utilizes the TDMM mechanism that we proposed and integrates impact-resistant magnetic joint fingers. The TDMM mechanism enables the MuxHand to control 9 DOF across its three fingers using only 4 motors, greatly reducing both the system's cost and volume. A series of experiments were conducted to validate MuxHand's performance. The results show that, through the TDMM mechanism and decoupled magnetic joints, the MuxHand achieves robust grasping and dexterous manipulation. The maximum load of a single finger reaches 7.0 kg, the maximum load at the finger joint root reaches 12.0 kg, the maximum driving load at the joint root is 5.0 kg, and the maximum driving load at the fingertip is 1.0 kg, while maintaining force even in a power-off state. The magnetic joints enhance durability, enabling the fingers to withstand external forces and impacts without damage.

However, this work still has some limitations. Further engineering optimizations were not explored, such as using motors with higher power density and torque to improve grasping force and load capacity. The impact of cable friction on grasping force and manipulation was also not discussed. We plan to address these limitations through further optimizations and research to enhance the grasping and manipulation performance of MuxHand. We hope that this work will contribute to future research on the miniaturization and cost reduction of cable-driven systems and dexterous hand systems.

## References

[1] S. Li, X. Yin, C. Xia, L. Ye, X. Wang, and B. Liang, "Tata: A universal jamming gripper with high-quality tactile perception and its application to underwater manipulation," in *International Conference on Robotics and Automation (ICRA)*, pp. 6151–6157, 2022.

[2] S. Li, L. Ye, C. Xia, X. Wang, and B. Liang, "Design of a tactile sensing robotic gripper and its grasping method," in *IEEE International Conference on Systems, Man, and Cybernetics (SMC)*, pp. 894–901, 2021.

[3] M. A. Armada, P. de González Santos, D. Alba, M. Armada, and R. Ponticelli, "An introductory revision to humanoid robot hands," in *Climbing and Walking Robots: Proceedings of the 7th International Conference CLAWAR 2004*, pp. 701–712, 2005.

[4] H. Liu, K. Wu, P. Meusel, N. Seitz, G. Hirzinger, M. Jin, Y. Liu, S. Fan, T. Lan, and Z. Chen, "Multisensory five-finger dexterous hand: The dlr/hit hand ii," in *IEEE/RSJ International Conference on Intelligent Robots and Systems*, pp. 3692–3697, 2008.

[5] U. Kim, D. Jung, H. Jeong, J. Park, H. Jung, J. Cheong, H. Choi, H. Do, and C. Park, "Integrated linkage-driven dexterous anthropomorphic robotic hand nat," *Commun*, vol. 12, no. 7177, pp. 10–1038, 2021.

[6] Y.-J. Kim, Y. Lee, J. Kim, J.-W. Lee, K.-M. Park, K.-S. Roh, and J.-Y. Choi, "Roboray hand: A highly backdrivable robotic hand with sensorless contact force measurements," in *IEEE International Conference on Robotics and Automation (ICRA)*, pp. 6712–6718, 2014.

[7] L. B. Bridgwater, C. A. Ihrke, M. A. Diftler, M. E. Abdallah, N. A. Radford, J. M. Rogers, S. Yayathi, R. S. Askew, and D. M. Linn, "The robonaut 2 hand - designed to do work with tools," in *2012 IEEE International Conference on Robotics and Automation (ICRA)*, pp. 3425–3430, 2012.

[8] S. Jacobsen, E. Iversen, D. Knutti, R. Johnson, and K. Biggers, "Design of the utah/m.i.t. dextrous hand," in *Proceedings. 1986 IEEE International Conference on Robotics and Automation*, vol. 3, pp. 1520–1532, 1986.

[9] S. R. Company, "Dexterous hand series." `https://www.shadowrobot.com/dexterous-hand-series/`, 2020.

[10] G. P. Kontoudis, M. V. Liarokapis, A. G. Zisimatos, C. I. Mavrogiannis, and K. J. Kyriakopoulos, "Open-source, anthropomorphic, underactuated robot hands with a selectively lockable differential mechanism: Towards affordable prostheses," in *2015 IEEE/RSJ International conference on intelligent robots and systems (IROS)*, pp. 5857–5862, IEEE, 2015.

[11] M. Baril, T. Laliberté, C. Gosselin, and F. Routhier, "On the design of a mechanically programmable underactuated anthropomorphic prosthetic gripper," *Journal of Mechanical Design*, vol. 135, no. 12, p. 121008, 2013.

[12] Y.-J. Kim, J. Yoon, and Y.-W. Sim, "Fluid lubricated dexterous finger mechanism for human-like impact absorbing capability," *IEEE Robotics and Automation Letters*, vol. 4, no. 4, pp. 3971–3978, 2019.

[13] Y. Zhu, G. Wei, L. Ren, Z. Luo, and J. Shang, "An anthropomorphic robotic finger with innate human-finger-like biomechanical advantages part ii: Flexible tendon sheath and grasping demonstration," *IEEE Transactions on Robotics*, vol. 39, no. 1, pp. 505–520, 2022.

[14] B.-Y. Sun, X. Gong, J. Liang, W.-B. Chen, Z.-L. Xie, C. Liu, and C.-H. Xiong, "Design principle of a dual-actuated robotic hand with anthropomorphic self-adaptive grasping and dexterous manipulation abilities," *IEEE Transactions on Robotics*, vol. 38, no. 4, pp. 2322–2340, 2021.

[15] J. Yan, H. Zheng, F. Sun, H. Liu, Y. Song, and B. Fang, "C-shaped bidirectional stiffness joint design for anthropomorphic hand," *IEEE Robotics and Automation Letters*, vol. 7, no. 4, pp. 12371–12378, 2022.

[16] C. Della Santina, C. Piazza, G. Grioli, M. G. Catalano, and A. Bicchi, "Toward dexterous manipulation with augmented adaptive synergies: The pisa/iit softhand 2," *IEEE Transactions on Robotics*, vol. 34, no. 5, pp. 1141–1156, 2018.

[17] G. Gao, A. Dwivedi, and M. Liarokapis, "The new dexterity adaptive humanlike robot hand: Employing a reconfigurable palm for robust grasping and dexterous manipulation," in *IEEE International Conference on Robotics and Automation (ICRA)*, pp. 10310–10316, 2023.

[18] R. R. Ma, L. U. Odhner, and A. M. Dollar, "A modular, open-source 3d printed underactuated hand," in *2013 IEEE International Conference on Robotics and Automation*, pp. 2737–2743, IEEE, 2013.

[19] V. H. Sundaram, R. Bhirangi, M. E. Rentschler, A. Gupta, and T. Hellebrekers, "Dragonclaw: A low-cost pneumatic gripper with integrated magnetic sensing," in *2023 IEEE International Conference on Soft Robotics (RoboSoft)*, pp. 1–8, IEEE, 2023.

[20] R. L. Truby, R. K. Katzschmann, J. A. Lewis, and D. Rus, "Soft robotic fingers with embedded ionogel sensors and discrete actuation modes for somatosensitive manipulation," in *2019 2nd IEEE international conference on soft robotics (RoboSoft)*, pp. 322–329, IEEE, 2019.

[21] G. Salvietti, Z. Iqbal, I. Hussain, D. Prattichizzo, and M. Malvezzi, "The co-gripper: a wireless cooperative gripper for safe human robot interaction," in *2018 IEEE/RSJ International Conference on Intelligent Robots and Systems (IROS)*, pp. 4576–4581, IEEE, 2018.

[22] I. Hussain, Z. Iqbal, M. Malvezzi, D. Prattichizzo, and G. Salvietti, "How to 3d-print compliant joints with a selected stiffness for cooperative underactuated soft grippers," in *Human-Friendly Robotics 2019: 12th International Workshop*, pp. 139–153, Springer, 2020.

[23] A. Pagoli, F. Chapelle, J. A. Corrales, Y. Mezouar, and Y. Lapusta, "A soft robotic gripper with an active palm and reconfigurable fingers for fully dexterous in-hand manipulation," *IEEE Robotics and Automation Letters*, vol. 6, no. 4, pp. 7706–7713, 2021.

[24] M. Dragusanu, G. M. Achilli, M. C. Valigi, D. Prattichizzo, M. Malvezzi, and G. Salvietti, "The wavejoints: a novel methodology to design soft-rigid grippers made by monolithic 3d printed fingers with adjustable joint stiffness," in *2022 International Conference on Robotics and Automation (ICRA)*, pp. 6173–6179, IEEE, 2022.

[25] C. Tawk, Y. Gao, R. Mutlu, and G. Alici, "Fully 3d printed monolithic soft gripper with high conformal grasping capability," in *2019 IEEE/ASME International Conference on Advanced Intelligent Mechatronics (AIM)*, pp. 1139–1144, IEEE, 2019.

[26] S. Liu, F. Wang, Z. Liu, W. Zhang, Y. Tian, and D. Zhang, "A two-finger soft-robotic gripper with enveloping and pinching grasping modes," *IEEE/ASME Transactions on Mechatronics*, vol. 26, no. 1, pp. 146–155, 2020.

[27] M. Dragusanu, S. Marullo, M. Malvezzi, G. M. Achilli, M. C. Valigi, D. Prattichizzo, and G. Salvietti, "The dressgripper: A collaborative gripper with electromagnetic fingertips for dressing assistance," *IEEE Robotics and Automation Letters*, vol. 7, no. 3, pp. 7479–7486, 2022.

[28] B. Koh and C. Chiang, "Radiated emission and signal integrity analysis on the folded flexible printed circuit cable," in *Asia-Pacific International Symposium on Electromagnetic Compatibility (APEMC)*, vol. 1, pp. 338–340, 2016.

[29] C. Knospe, "Pid control," *IEEE Control Systems Magazine*, vol. 26, no. 1, pp. 30–31, 2006.

[30] J. K. Lee, C. H. Choi, K. H. Yoon, H. J. Lee, B. S. Park, and J. S. Yoon, "Design and evaluation of cable-driven manipulator with motion-decoupled joints," in *International Conference on Smart Manufacturing Application*, pp. 575–580, 2008.

[31] K. Tan, H. Shi, X. Mei, T. Geng, and J. Yang, "Control of force transmission for cable-driven actuation system based on modified friction model with compensation parameters," *Control Engineering Practice*, vol. 151, p. 106035, 2024.

[32] L. Radulovic and Z. Wojcinski, "Ptfe (polytetrafluoroethylene; teflon®)," in *Encyclopedia of Toxicology (Third Edition)* (P. Wexler, ed.), pp. 1133–1136, Oxford: Academic Press, third edition ed., 2014.

[33] S. Cobos, M. Ferre, M. A. Sánchez-Urán, and J. Ortego, "Constraints for realistic hand manipulation," *Proc. Presence*, vol. 2007, pp. 369–370, 2007.

[34] B. Calli, A. Walsman, A. Singh, S. Srinivasa, P. Abbeel, and A. M. Dollar, "Benchmarking in manipulation research: Using the yale-cmu-berkeley object and model set," *IEEE Robotics & Automation Magazine*, vol. 22, no. 3, pp. 36–52, 2015.